AIAA JOURNAL
Vol. 56, No. 11, November 2018

Analysis of the Aerodynamic Benefit from Boundary Layer Ingestion for Transport Aircraft

Alejandra Uranga*
University of Southern California, Los Angeles, California 90089
and
Mark Drela,† David K. Hall,‡ and Edward M. Greitzer§
Massachusetts Institute of Technology, Cambridge, Massachusetts 02139

DOI: 10.2514/1.J056781

Propulsors with boundary layer ingestion (BLI) generate a propulsive force with lower flow power input than conventional engines. This aerodynamic benefit can be traced back to its sources: reductions in jet, surface, and wake dissipation. A framework for BLI analysis is developed based on the power balance method: parametric expressions are derived for the net streamwise force on an aircraft and for the mechanical flow power required, as well as relations for the dissipation components. They illustrate the range of possible comparisons between BLI and non-BLI engine installations, and show how the benefit varies with design choices. Applying the framework to wind tunnel data from powered D8 aircraft model tests, the sources of aerodynamic BLI benefit are quantified for a realistic transport aircraft configuration. With the same propulsors (equal nozzle area) BLI reduces cruise power by 8.2%, of which 5.2% comes from a reduction in jet dissipation, 2.4% from reduced surface dissipation, and 0.6% from reduced wake dissipation. The jet dissipation reduction is equivalent to a 3.4 percentage points increase in propulsive efficiency. If the installations are compared at equal mass flow, the benefit amounts to a 9% lower cruise power.

Nomenclature

A	=	flow area
AR	=	aspect ratio, $\text{span}^2/S_{\text{ref}}$
C'_D	=	aircraft drag coefficient for non-BLI configuration, $D'/(q_\infty S_{\text{ref}})$
C_{D_i}	=	aircraft induced drag coefficient, $D_i/(q_\infty S_{\text{ref}})$
C'_{D_p}	=	aircraft profile drag coefficient for non-BLI configuration, $D'_p/(q_\infty S_{\text{ref}})$
C_L	=	vertical aerodynamic force (lift) coefficient, $F_L/(q_\infty S_{\text{ref}})$
C_{P_K}	=	mechanical flow power coefficient, $P_K/(q_\infty V_\infty S_{\text{ref}})$
$C_{P_{\text{sp}}}$	=	specific propulsive power, $(P_K - \Phi_{\text{jet}})/(\dot{m}V_\infty^2)$
C_X	=	net streamwise force coefficient, $F_X/(q_\infty S_{\text{ref}})$
C_{X_0}	=	net streamwise force coefficient at zero power, $C_X(C_{P_K} = 0)$
C_Φ	=	dissipation coefficient, $\Phi/(q_\infty V_\infty S_{\text{ref}})$
D'	=	aircraft drag for non-BLI configuration
D'_p	=	aircraft profile drag for non-BLI configuration
D_i	=	induced drag
e	=	span efficiency
F_X	=	net streamwise force; $F_X < 0$ indicates net forward force
F_L	=	vertical aerodynamic force (lift)
f_{BLI}	=	fraction of airframe's surface boundary layer kinetic energy defect ingested by propulsors
f_{wake}	=	fraction of airframe's viscous (nonvortex) dissipation that occurs in the wake, $\Phi_{\text{wake}}/(\Phi_{\text{wake}} + \Phi_{\text{surf}})$
$\dot{m}$	=	mass flow through propulsors, $N_{\text{prop}}\rho_{\text{jet}}V_{\text{jet}}A_{\text{jet}}$
N_{prop}	=	number of propulsors
$\hat{\boldsymbol{n}}$	=	unit normal vector
P_K	=	mechanical flow power
P_V	=	volumetric flow power
PSC	=	power saving coefficient, $(P'_K - P_K)/P'_K$
p	=	static pressure
q_∞	=	freestream dynamic pressure, $(1/2)\rho_\infty V_\infty^2$
S_{ref}	=	reference area
$\mathcal{S}$	=	surface of body, including propulsor inlet and outlet
U_{tip}	=	fan blade tip speed
V	=	velocity magnitude (speed), $\lvert\boldsymbol{V}\rvert$
$\boldsymbol{V}$	=	velocity vector
$\Delta C_{\Phi_{\text{surf}}}$	=	surface dissipation coefficient change from non-BLI to BLI configuration, $C'_{\Phi_{\text{surf}}} - C_{\Phi_{\text{surf}}}$
$\Delta\Phi_{\text{surf}}$	=	surface dissipation change from non-BLI to BLI configuration, $\Phi'_{\text{surf}} - \Phi_{\text{surf}}$
η_p	=	propulsive efficiency, $(P_K - \Phi_{\text{jet}})/P_K$
ρ	=	density
$\bar{\bar{\boldsymbol{\tau}}}$	=	viscous stress tensor
ϕ	=	propulsor flow coefficient, $V_{\text{fan}}/U_{\text{tip}}$
Φ	=	dissipation
Φ_∞	=	total viscous dissipation, $\Phi_{\text{surf}} + \Phi_{\text{wake}} + \Phi_{\text{vortex}} + \Phi_{\text{jet}}$

Subscripts

$()_{\text{airframe}}$	=	airframe quantity from unpowered configuration
$()_{\text{fan}}$	=	propulsor fan face quantity
$()_{\text{jet}}$	=	propulsor jet quantity
$()_{\text{nozzle}}$	=	propulsor nozzle quantity
$()_{\text{prop}}$	=	propulsor quantity
$()_{\text{surf}}$	=	surface quantity
$()_{\text{vortex}}$	=	vortex quantity
$()_{\text{wake}}$	=	wake quantity
$()_\infty$	=	freestream (flight) quantity

Superscript

$()'$	=	quantity of non-BLI configuration

Received 2 October 2017; revision received 20 March 2018; accepted for publication 7 June 2018; published online Open Access 28 September 2018.

*Assistant Professor, Department of Aerospace and Mechanical Engineering (formerly Research Engineer at MIT), 854 Downey Way RRB 218; auranga@usc.edu. Senior Member AIAA.
†Terry J. Kohler Professor of Fluid Dynamics, Department of Aeronautics and Astronautics. Fellow AIAA.
‡Research Engineer. Member AIAA.
§H.N. Slater Professor of Aeronautics and Astronautics, Honorary. Fellow AIAA.

I. Introduction

THE increased demand for air transportation and the growing emphasis on environmental sustainability have led to enhanced interest in fuel efficiency. Boundary layer ingestion (BLI)—with which at least part of the airframe's boundary layer or wake is ingested by the propulsion system—has the potential to provide step improvements in fuel consumption and has been proposed for a number of advanced subsonic transport aircraft concepts, including hybrid and blended wing bodies [1,2], aircraft with distributed propulsion [3,4], NASA's STARC-ABL concept [5], and the D8 double-bubble [6–9].

The advantageous effects of BLI for transport aircraft can be classified as follows:

1) Reduced propulsor jet dissipation for a given force and therefore increased propulsive efficiency (a lower propulsor power is thus required to obtain the same net streamwise force)

2) Reduced surface dissipation due to the smaller partially embedded nacelles, which see lower surface velocities

3) Reduced wake dissipation due to the propulsors partially eliminating the fuselage viscous wake

4) Reduced weight due to smaller nacelles and smaller engines (from the reduced power requirement), which in turn enables smaller wings, and thus an even lighter aircraft

The first three effects correspond to comparison of flight power requirements for a given airframe operating at the same lift coefficient and constitute what will be called the *aerodynamic* benefit of BLI. In a design setting, the airframe can be re-optimized to take full advantage of BLI, thus leading to the fourth benefit source, which is referred to as the *system-level* benefit. Experimental tests of the D8 configuration demonstrated an aerodynamic benefit from BLI of more than 8% [9], with a total system-level benefit estimated to be close to 19% [8,10].

To justify the increased complexity of using BLI, it is important to be able to predict the achievable performance gains, and to understand their physical origins. Building upon the power balance method [11] and its application to BLI [12], we focus on the aerodynamic benefit of BLI and derive parametric expressions for the aircraft's net streamwise force (drag minus thrust for a conventional aircraft) and for the associated propulsive power as functions of the airframe and propulsor parameters. A breakdown of the dissipation, or power consumption, sources is also given. These provide a framework for estimate performance gains from BLI.

The methodology is applied to experimental data obtained on a 1:11 scale powered model of the D8 aircraft tested in the NASA Langley 14- by 22-Foot Subsonic Tunnel with back-to-back non-BLI and BLI configurations [9]. The sources of the aerodynamic BLI benefit are thus quantified for a realistic transport aircraft configuration. The different bases of comparison of BLI and non-BLI systems are illustrated, and it is shown how the benefit varies for different design choices.

II. Boundary Layer Ingestion

A. Overview

In a conventional engine installation, the propulsors are mounted away from the aircraft's body in order to minimize any adverse interaction between propulsors and airframe. The propulsors ingest uniform freestream flow and their jets counteract the momentum defect in the airframe wake. At cruise, the jets and wakes combine to a zero net momentum, but both the airframe's boundary layer (or its extension, the wake) and the propulsor's jet represent wasted kinetic energy—proportional to the square of the velocity difference between wake or jet and freestream.

An alternative way to achieve a zero net momentum is to place the propulsors in the boundary layer of the airframe, and thus re-energize the slower-moving flow, which otherwise forms the wake. This produces a combined wake and jet with lower kinetic energy, and therefore lower losses, than a conventional propulsor. This ingestion of at least part of the airframe's (fuselage and/or wings) boundary layer by the propulsors, called *boundary layer ingestion* or BLI, increases the overall efficiency of the system.

Traditional force accounting methods are well suited to study aircraft without BLI, for which the interaction between airframe and propulsors is minimal. The subsystems can be studied in isolation, and small corrections made to the superposition of the two to account for installation effects. Such methods have been used for the design of aircraft for decades.

On the other hand, the interaction between propulsors and airframe is a prime characteristic of BLI, and the classical notions of thrust and drag—defined by separate, nonoverlapping control volumes encompassing either the propulsors or the airframe—become ambiguous. Thus, although the theoretical benefit of BLI has been known since the 1940s [13] and been the subject of several theoretical studies [14,15], analysis and design of BLI systems is still a field of active research.

The analysis of aircraft configurations with integrated airframe-propulsion systems, such as those occurs with BLI, are well described using the power balance method [11]. A summary of the elements of this method that are relevant to the present study is presented next, and then used for the derivations of the proposed framework in Sec. III.

B. Power Balance Analysis

The power balance is formulated on a control volume $\mathcal{V}$ with inner boundary $\mathcal{S}$ covering the body surface and spanning the propulsor inlet and exit planes, and an outer boundary effectively at infinity, as shown in Fig. 1. The boundary has a unit normal $\hat{\boldsymbol{n}}$ defined out of the flow volume and therefore into the body.

The power balance for this volume, assuming steady flow, is

$$F_X V_\infty = \Phi_\infty - P_K - P_V \tag{1}$$

where V_∞ is the freestream speed, and the rest of the terms are defined next. The net streamwise force component, F_X, on the body including the propulsors, is defined via

$$F_X V_\infty \equiv \oiint_{\mathcal{S}} \left[(p - p_\infty)\hat{\boldsymbol{n}} - \bar{\bar{\boldsymbol{\tau}}} \cdot \hat{\boldsymbol{n}} + \rho \boldsymbol{V}(\boldsymbol{V} \cdot \hat{\boldsymbol{n}}) \right] \cdot \boldsymbol{V}_\infty \, \mathrm{d}\mathcal{S} \tag{2}$$

which is the traditional accounting of pressure differences $(p - p_\infty)$ and shear stresses $\bar{\bar{\boldsymbol{\tau}}}$ over the surface of the whole body, and of momentum flux. Here ρ is the flow's density, $\boldsymbol{V}$ its velocity vector (of magnitude V), and $\boldsymbol{V}_\infty$ the freestream velocity vector (of magnitude V_∞).

The net mechanical flow power passing through the propulsor inlet and exit is

$$P_K \equiv \oiint_{\mathcal{S}} \left[p_\infty - p + \frac{1}{2}\rho(V_\infty^2 - V^2) \right] \boldsymbol{V} \cdot \hat{\boldsymbol{n}} \, \mathrm{d}\mathcal{S} \tag{3}$$

It is defined only on the propulsor inlet and exit planes, and thus does not depend on fan performance characteristics, efficiency, or distortion response: losses internal to the propulsor are immaterial to its effect on the external flowfield. Mechanical flow power is thus used as the performance metric for the comparison of configurations with and without BLI and as a surrogate for fuel burn.

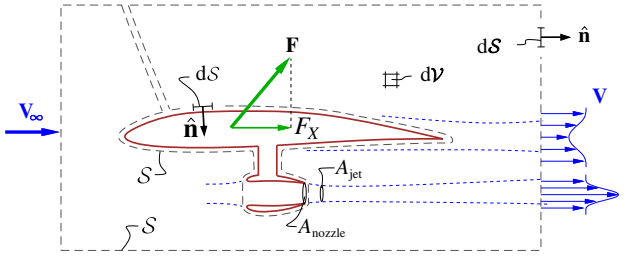

Fig. 1 Control volume $\mathcal{V}$ and its surface $\mathcal{S}$ used for the power balance analysis. F_X is the streamwise component of the net force, $\boldsymbol{F}$, on the body.

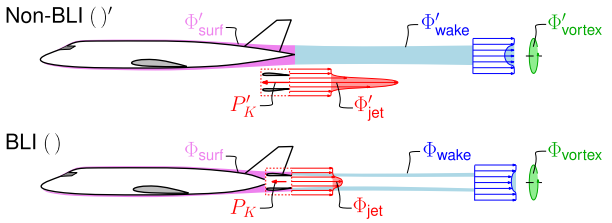

Fig. 2 Illustration of power-balance terms for conventional (top) and boundary layer ingesting aircraft (bottom).

The volumetric flow power,

$$P_V \equiv \iiint (p - p_\infty)\nabla \cdot \boldsymbol{V}\, \mathrm{d}\mathcal{V} \tag{4}$$

is a "$p\mathrm{d}v$" power that is zero for incompressible flow. For compressible flow, neglecting P_V is a good approximation due to various cancellations that occur in the formulation. Any isentropic streamtubes that start and end at freestream have zero net contribution to P_V. This is also the case for the streamtube that enters a non-BLI propulsor (extending from freestream to propulsor inlet). The streamtube that exits the propulsor has a negligible contribution to the overall P_V if it is taken to start just downstream of the propulsor where the jet pressure has reached atmospheric pressure ($p \simeq p_\infty$) but no significant dissipation has yet taken place. This again is a good approximation, because a significantly under- or overexpanded supersonic jet generally does not occur on transport aircraft with modern low fan-pressure-ratio engines. Thus, the only nonzero contribution to the volumetric flow power occurs inside compressible boundary layers where $\nabla \cdot \boldsymbol{V} \neq 0$, and this contribution can be quantified via a small correction to the surface dissipation, less than 5% for typical transonic flows [16]. Furthermore, these assumptions impact both BLI and non-BLI configurations nearly equally, and hence does not affect the BLI benefit. We will therefore assume that $P_V \simeq 0$ throughout this work, but hold that the relations remain excellent approximations even for compressible flows.

The total viscous dissipation within the control volume is

$$\Phi_\infty \equiv \iiint (\bar{\bar{\tau}} \cdot \nabla) \cdot \boldsymbol{V}\, \mathrm{d}\mathcal{V} \tag{5}$$

$$= \Phi_{\text{surf}} + \Phi_{\text{wake}} + \Phi_{\text{vortex}} + \Phi_{\text{jet}} \tag{6}$$

and is the sum of all the dissipation sources in the flowfield as illustrated in Fig. 2: surface, wake, vortex, and jet. These components are described and estimated next.

III. Analysis Framework

In this section, expressions for the dissipation components, the mechanical flow power, and the net streamwise force are derived based on the power balance method [11] with a quasi-one-dimensional model for the propulsor jet. They constitute a framework for the analysis of BLI aircraft. In what follows, a prime $()'$ indicates quantities and expressions that are only valid for a non-BLI configuration, whereas nonprimed quantities refer to general terms applicable both with and without BLI.

A. Dissipation Components

The breakdown of the BLI aerodynamic benefit into its sources can be done by computing the various dissipation components in Eq. (6), as follows. Dissipation terms are nondimensionalized by $(1/2)\rho_\infty V_\infty^3 S_{\text{ref}}$ (freestream dynamic pressure times velocity times reference area) to obtain the dissipation coefficients.

1. *Surface Dissipation*

For a non-BLI configuration with distinct airframe wakes and propulsive jets, it is possible to write the surface, wake, and vortex dissipations in terms of the—assumed known—conventional drag components. The total airframe dissipation and total drag D' are related via

$$\Phi'_{\text{surf}} + \Phi'_{\text{wake}} + \Phi'_{\text{vortex}} = D' V_\infty \tag{7}$$

Total drag can be decomposed into profile and induced parts,

$$D' = D'_p + D'_i \tag{8}$$

and vortex dissipation is the same as induced drag power,

$$\Phi'_{\text{vortex}} = D'_i V_\infty \tag{9}$$

such that the combined surface + wake dissipation is the profile drag power:

$$\Phi'_{\text{surf}} + \Phi'_{\text{wake}} = D'_p V_\infty \tag{10}$$

To separate losses that occur along the surface from those in the wake, the fraction of the airframe's nonvortex dissipation occurring in the wake is defined as

$$f_{\text{wake}} \equiv \frac{\Phi'_{\text{wake}}}{\Phi'_{\text{surf}} + \Phi'_{\text{wake}}} \tag{11}$$

Two-dimensional viscous flow calculations [17] show values of f_{wake} with well-attached turbulent flow typically falling between 0.08 and 0.14, while nearly separated flow near the trailing edge can have f_{wake} values of 0.30 or more.

From definition (11),

$$\Phi'_{\text{surf}} = (1 - f_{\text{wake}})(\Phi'_{\text{surf}} + \Phi'_{\text{wake}}) \tag{12}$$

and Eq. (10) gives

$$\Phi'_{\text{surf}} = (1 - f_{\text{wake}}) D'_p V_\infty \tag{13}$$

which is an expression for the surface dissipation of a non-BLI aircraft as a function of profile drag. In nondimensional form, it reads

$$C'_{\Phi_{\text{surf}}} = (1 - f_{\text{wake}}) C'_{D_p} \tag{14}$$

In the switch from a non-BLI engine installation to one with BLI, the total surface dissipation will likely change because BLI can enable smaller nacelles and eliminates pylons, but requires the addition of blending surfaces to integrate the propulsors into the airframe. The change in surface dissipation between a non-BLI system and one with BLI is defined as

$$\Delta\Phi_{\text{surf}} \equiv \Phi'_{\text{surf}} - \Phi_{\text{surf}} \tag{15}$$

Because the elimination of pylons and the smaller nacelle surfaces will reduce the total wetted area, it is expected that $\Delta\Phi_{\text{surf}} > 0$, reflecting one of the advantages of BLI. This also assumes that the upstream boundary layer dissipation is largely unaffected by the presence of the propulsors as verified by [12,16]. In practice, the value of $\Delta\Phi_{\text{surf}}$ will depend on the specifics of the particular engine-airframe integration being considered.

From definition (15) and expression (13), the surface dissipation of the BLI configuration can be written as

$$\Phi_{\text{surf}} = (1 - f_{\text{wake}}) D'_p V_\infty - \Delta\Phi_{\text{surf}} \tag{16}$$

or, in terms of coefficients,

$$C_{\Phi_{\text{surf}}} = (1 - f_{\text{wake}}) C'_{D_p} - \Delta C_{\Phi_{\text{surf}}} \tag{17}$$

2. Wake Dissipation

The wake dissipation of the non-BLI configuration can be written using Eq. (10) and definition (11) as

$$\Phi'_{\text{wake}} = f_{\text{wake}}(\Phi'_{\text{surf}} + \Phi'_{\text{wake}}) = f_{\text{wake}} D'_p V_\infty \tag{18}$$

or, in nondimensional form,

$$C'_{\Phi_{\text{wake}}} = f_{\text{wake}} C'_{D_p} \tag{19}$$

With BLI, the propulsors ingest a fraction, f_{BLI}, of the airframe's boundary layer kinetic energy defect. The wake dissipation is thus reduced by this ingestion fraction because that is also the fraction of kinetic energy defect removed from the wake at the trailing edge, such that

$$\Phi_{\text{wake}} = (1 - f_{\text{BLI}})\Phi'_{\text{wake}} \tag{20}$$

and therefore

$$\Phi_{\text{wake}} = (1 - f_{\text{BLI}}) f_{\text{wake}} D'_p V_\infty \tag{21}$$

which is nondimensionalized as

$$C_{\Phi_{\text{wake}}} = f_{\text{wake}}(1 - f_{\text{BLI}}) C'_{D_p} \tag{22}$$

3. Vortex Dissipation

In nondimensional form, Eq. (9) states that the vortex dissipation coefficient is equal to the traditional induced drag coefficient, $C_{\Phi_{\text{vortex}}} = C_{D_i}$. It can thus be written as

$$C_{\Phi_{\text{vortex}}} = \frac{C_L^2}{\pi AR e} \tag{23}$$

in terms of lift coefficient C_L, aspect ratio AR, and span efficiency e, with a similar expression for the non-BLI case. Note that induced drag is well defined even with BLI, as long as the propulsive jets and viscous wakes are compact compared with the overall transverse potential flow associated with the trailing vorticity.

As stated in the introduction, the aerodynamic benefit corresponds to a given airframe and lift coefficient, that is, $AR' = AR$ and $C_L = C'_L$. If the BLI installation is designed so as to not affect the lift distribution, then the span efficiency is also unchanged and hence $C_{\Phi_{\text{vortex}}} = C'_{\Phi_{\text{vortex}}}$. If, on the other hand, the presence of BLI propulsors changes the lift magnitude and/or its distribution, then the change in vortex dissipation for the specific airframe-propulsion integration needs to be quantified.

4. Jet Dissipation

The jet dissipation is equal to the kinetic energy deposition [11],

$$\Phi_{\text{jet}} = \iint_{\text{exit}} \frac{1}{2}(V - V_\infty)^2 \, \mathrm{d}\dot{m} \tag{24}$$

where the integral is carried out over the mass flow through the propulsor exit. Assuming uniform velocity V_{jet} across the jet is an excellent approximation because the jet total pressure nonuniformity is much smaller than the pressure rise imparted by the propulsor as examined in [12]. The jet dissipation can then be computed as

$$\Phi_{\text{jet}} = \frac{1}{2}(V_{\text{jet}} - V_\infty)^2 \dot{m} \tag{25}$$

using the total mass flow through the propulsors

$$\dot{m} = N_{\text{prop}} \rho_{\text{jet}} V_{\text{jet}} A_{\text{jet}} \tag{26}$$

in which N_{prop} is the number of propulsors and the subscript $()_{\text{jet}}$ refers to quantities at the location—a short distance downstream of the propulsor nozzle exit plane—where the jet has reached freestream pressure ($p_{\text{jet}} \simeq p_\infty$), but no significant dissipation has yet taken place. This is consistent with the isolated-propulsor force analysis assumption that the jet reaches ambient pressure before any significant mixing has occurred.

The jet dissipation is thus given by

$$\Phi_{\text{jet}} = \frac{1}{2}(V_{\text{jet}} - V_\infty)^2 N_{\text{prop}} \rho_{\text{jet}} V_{\text{jet}} A_{\text{jet}} \tag{27}$$

and its nondimensional coefficient by

$$C_{\Phi_{\text{jet}}} = N_{\text{prop}} \left(\frac{V_{\text{jet}}}{V_\infty} - 1 \right)^2 \frac{\rho_{\text{jet}}}{\rho_\infty} \frac{V_{\text{jet}}}{V_\infty} \frac{A_{\text{jet}}}{A_{\text{nozzle}}} \frac{A_{\text{nozzle}}}{S_{\text{ref}}} \tag{28}$$

where A_{nozzle} is the propulsor nozzle area, A_{jet} the area of the jet where it reaches freestream pressure, and S_{ref} the configuration reference area. This expression is valid for both BLI and non-BLI cases, with the latter using the corresponding ρ'_{jet}, V'_{jet}, A'_{jet}.

B. Mechanical Flow Power

The mechanical flow power defined by the surface integral (3) can be broken into fluxes at the exit and at the inlet of the propulsor as

$$P_K = \iint_{\text{exit}} \left(\frac{p - p_\infty}{\rho} + \frac{V^2 - V_\infty^2}{2} \right) \mathrm{d}\dot{m} - \iint_{\text{inlet}} \left(\frac{p - p_\infty}{\rho} + \frac{V^2 - V_\infty^2}{2} \right) \mathrm{d}\dot{m} \tag{29}$$

Assuming again uniform velocity V_{jet} across the jet, the exit integral becomes

$$\begin{aligned} P_{K_{\text{exit}}} &= \frac{1}{2}(V_{\text{jet}}^2 - V_\infty^2)\dot{m} \\ &= \frac{1}{2}(V_{\text{jet}}^2 - V_\infty^2) N_{\text{prop}} \rho_{\text{jet}} V_{\text{jet}} A_{\text{jet}} \end{aligned} \tag{30}$$

The inlet integrand in Eq. (29) is seen to be the incompressible total pressure defect, and is zero in the absence of BLI. It would remain zero for a compressible flow if the P_V term is retained.

With BLI, the propulsor ingests a fraction of the total surface dissipation in the boundary layer upstream of the propulsors, and so the inlet integral can be written as

$$P_{K_{\text{inlet}}} = -f_{\text{BLI}} \Phi'_{\text{surf}} \tag{31}$$

Note that Φ'_{surf} is used here because any changes in surface dissipation due to the BLI installation ($\Delta\Phi_{\text{surf}}$) will be outside of the ingested streamtube. Equation (29) then becomes

$$P_K = \frac{1}{2}(V_{\text{jet}}^2 - V_\infty^2) N_{\text{prop}} \rho_{\text{jet}} V_{\text{jet}} A_{\text{jet}} + f_{\text{BLI}} \Phi'_{\text{surf}} \tag{32}$$

which is applicable to both BLI and non-BLI configurations, with $f_{\text{BLI}} = 0$ for the latter. The jet velocity can be different for the two configurations depending on how the comparison is being made. The jet area is a priori unknown, but in practice it will be close to the known nozzle area A_{nozzle}.

C. Streamwise Force

Writing the power balance equation (1) as

$$F_X V_\infty = (\Phi_{\text{surf}} + \Phi_{\text{wake}} + \Phi_{\text{vortex}}) - (P_K - \Phi_{\text{jet}}) \tag{33}$$

using Eqs. (27) and (32) to eliminate Φ_{jet} and P_K, and dividing by V_∞, gives an expression for the streamwise force

$$F_X = (\Phi_{\text{surf}} + \Phi_{\text{wake}} + \Phi_{\text{vortex}})/V_\infty - f_{\text{BLI}}\Phi'_{\text{surf}}/V_\infty - (V_{\text{jet}} - V_\infty)N_{\text{prop}}\rho_{\text{jet}}V_{\text{jet}}A_{\text{jet}} \tag{34}$$

Note that a negative F_X corresponds to a net forward force, and the above equation shows that even with the same jet velocity and airframe dissipation ($\Phi_{\text{surf}} + \Phi_{\text{wake}} + \Phi_{\text{vortex}}$), BLI provides a forward-force advantage of $f_{\text{BLI}}\Phi_{\text{surf}}/V_\infty$. Similarly, the flow power equation (32) shows that BLI has the effect of adding $f_{\text{BLI}}\Phi_{\text{surf}}$ more power to the flow.

D. Explicit Parametric Expressions

Expressions (32) and (34) can be recast in terms of the conventional drag components of the non-BLI airframe alone, to provide a way to explicitly quantify the BLI benefit in terms of airframe parameters, propulsor parameters, and the ingestion fraction.

Introducing expressions (16) and (20) for surface and wake dissipation, taking $\Phi_{\text{vortex}} = \Phi'_{\text{vortex}}$, and using the dissipation-drag relation (7), the expressions (32) and (34) for mechanical flow power and streamwise force become

$$P_K = \frac{1}{2}(V_{\text{jet}}^2 - V_\infty^2)N_{\text{prop}}\rho_{\text{jet}}A_{\text{jet}}V_{\text{jet}} + (1 - f_{\text{wake}})f_{\text{BLI}}D'_pV_\infty \tag{35}$$

$$F_X = D' - f_{\text{BLI}}D'_p - \Delta\Phi_{\text{surf}}/V_\infty - (V_{\text{jet}} - V_\infty)N_{\text{prop}}\rho_{\text{jet}}V_{\text{jet}}A_{\text{jet}} \tag{36}$$

Nondimensionalizing by $(1/2)\rho_\infty V_\infty^3 S_{\text{ref}}$ and $(1/2)\rho_\infty V_\infty^2 S_{\text{ref}}$, respectively, gives the corresponding power and force coefficients

$$C_{P_K} = N_{\text{prop}}\left[\left(\frac{V_{\text{jet}}}{V_\infty}\right)^2 - 1\right]\frac{\rho_{\text{jet}}}{\rho_\infty}\frac{V_{\text{jet}}}{V_\infty}\frac{A_{\text{jet}}}{A_{\text{nozzle}}}\frac{A_{\text{nozzle}}}{S_{\text{ref}}} + (1 - f_{\text{wake}})f_{\text{BLI}}C'_{D_p} \tag{37}$$

$$C_X = C'_D - f_{\text{BLI}}C'_{D_p} - \Delta C_{\Phi_{\text{surf}}} - 2N_{\text{prop}}\left(\frac{V_{\text{jet}}}{V_\infty} - 1\right)\frac{\rho_{\text{jet}}}{\rho_\infty}\frac{V_{\text{jet}}}{V_\infty}\frac{A_{\text{jet}}}{A_{\text{nozzle}}}\frac{A_{\text{nozzle}}}{S_{\text{ref}}} \tag{38}$$

The jet flow properties ($\rho_{\text{jet}}, A_{\text{jet}}, V_{\text{jet}}$) with BLI may differ from the corresponding values ($\rho'_{\text{jet}}, A'_{\text{jet}}, V'_{\text{jet}}$) without BLI. The jet area ratio $A_{\text{jet}}/A_{\text{nozzle}}$ represents the jet contraction between the nacelle trailing edge (nozzle exit) and the location where the jet reaches freestream pressure, and is typically close to unity.

The parametric expressions (37) and (38) are valid both with and without BLI, and are explicit in the sense that they are expressed in terms of the—a priori known—total and profile drag of the non-BLI configuration. They identify and quantify the effects of the following major design parameters for a BLI system:

1) the ingested dissipation $f_{\text{BLI}}C'_{D_p}$, or simply the ingestion fraction f_{BLI} if the airframe is common to both configurations;

2) how efficient the BLI engine installation is, as quantified by $\Delta\Phi_{\text{surf}}$;

3) the propulsor operating points for each of the configurations, as indicated by the jet velocities V'_{jet}/V_∞ and V_{jet}/V_∞, or alternatively the corresponding mass flows.

Two important points are worth noting. First, the quantities f_{BLI} and C'_{D_p} always appear together as a factor, and thus are considered together as a single parameter. This reflects the fact that the ingested dissipation is the relevant physical quantity. For instance, an airframe with high dissipation (large C'_{D_p}) and propulsors that only ingest a small fraction of it (small f_{BLI}) may see a similar BLI benefit as a streamlined airframe with propulsors ingesting most of its boundary layer (small C'_{D_p} but high f_{BLI}).

Second, as long as the flow over the airframe is not drastically changed by the presence of ingesting propulsors and the nozzle is well designed to expand the jet flow to nearly atmospheric pressure, the parameters f_{wake}, $A_{\text{jet}}/A_{\text{nozzle}}$, and $A'_{\text{jet}}/A'_{\text{nozzle}}$ will not have a strong influence on the performance difference with and without BLI.

E. Performance Metrics

1. Power-Saving Coefficient and Power Ratio

BLI reduces the propulsor flow power required to achieve a certain net streamwise force, as quantified by the $C_{P_K}(C_X)$ functions parametrically defined by expressions (37) and (38). The aerodynamic BLI benefit can be quoted as either the power saving coefficient

$$\text{PSC} = \frac{C'_{P_K}(C'_X) - C_{P_K}(C_X)}{C'_{P_K}(C'_X)} \tag{39}$$

which is analogous to the expression used by Smith [14], or as the mechanical flow power ratio, P_K/P'_K, with the comparison done at the same net streamwise force $C_X = C'_X$.

2. Propulsive Efficiency

The propulsive efficiency is defined as the ratio of net propulsive power to mechanical power added to the flow. In terms of power-balance quantities, it is given by

$$\eta_p \equiv \frac{P_K - \Phi_{\text{jet}}}{P_K} = \frac{C_{P_K} - C_{\Phi_{\text{jet}}}}{C_{P_K}} \tag{40}$$

and can be calculated via Eqs. (28) and (37) for jet dissipation and flow power, respectively. This η_p definition is consistent with the conventional Froude efficiency [18], because for an isolated propulsor $P_K - \Phi_{\text{jet}}$ is the thrust power and $P_K = (1/2)\dot{m}(V_{\text{jet}}^2 - V_\infty^2)$. Definition (40), however, applies directly to both conventional and BLI propulsion systems, and is always less than unity.

3. Specific Propulsive Power

Instead of specific thrust, a more appropriate quantity in the presence of BLI is the specific propulsive power

$$C_{P_{\text{sp}}} \equiv \frac{P_K - \Phi_{\text{jet}}}{\dot{m}V_\infty^2} = \frac{V_{\text{jet}}}{V_\infty} - 1 + (1 - f_{\text{wake}})f_{\text{BLI}}\frac{D'_p}{\dot{m}V_\infty} \tag{41}$$

For a non-BLI configuration, this expression reduces to the conventional specific thrust $V_{\text{jet}}/V_\infty - 1$. Since $\eta_P P_K = P_K - \Phi_{\text{jet}}$, a useful relation between propulsive efficiency and specific propulsive power is

$$C_{P_{\text{sp}}} = \eta_p\frac{P_K}{\dot{m}V_\infty^2} \tag{42}$$

IV. Application to a BLI Aircraft

The analysis framework derived in Sec. III is now applied to wind tunnel test data for the D8 transonic transport concept, which takes advantage of boundary layer ingesting engines that are flush-mounted on the top aft fuselage. Here the measured aerodynamic benefit of the D8 BLI propulsion system is analyzed and quantitatively broken down into its sources.

A. Overview of Wind Tunnel Experiments

A back-to-back comparison of non-BLI and BLI versions of the D8 was conducted using 1 : 11 scale (4 m span) powered models in the NASA Langley 14- by 22-Foot Subsonic Tunnel during two test campaigns in 2013 and 2014 as part of the NASA/MIT $N + 3$ Phase 2 project. The major features of the wind tunnel experiments are summarized here; further details can be found in [9,10].

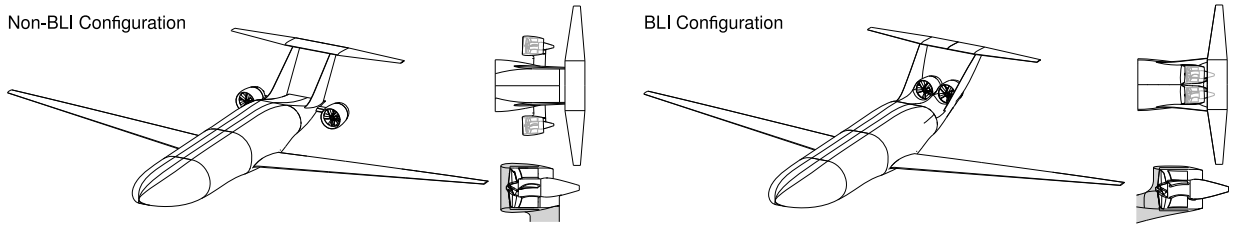

Fig. 3 D8 model in non-BLI (left) and BLI configurations (right). The third unpowered configuration is the same as the non-BLI model but with the propulsor nacelles and pylons removed.

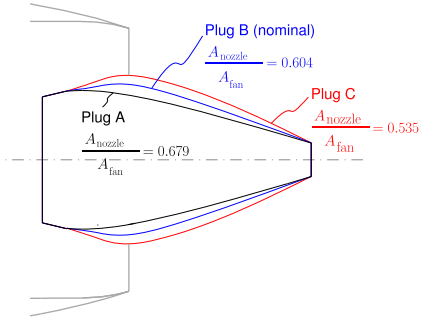

Fig. 4 Propulsor plugs and their corresponding nozzle areas.

1. *D8 Model Configurations*

The wind tunnel experiments were primarily designed to measure the aerodynamic benefit of BLI for the D8, which was tested under different configurations, shown in Fig. 3. The wind tunnel model is an 11:1 scaled version of the full-scale D8.2 aircraft, which is a conceptual design using aluminum materials and 2010-level engine technology. The *non-BLI configuration*, serving as the reference baseline, has podded propulsors with axisymmetric nacelles that are mounted on pylons at the rear of the aircraft and ingest freestream flow. The *BLI configuration* has propulsors embedded in the aft upper fuselage to ingest part of the airframe's boundary layer. A third *unpowered configuration*, with the propulsor nacelles and pylons removed, was also tested to quantify the airframe's aerodynamic characteristics.

To remove extraneous variability and facilitate comparison, the two configurations shared the same physical components, except for the removable aft 20% of the fuselage and attached vertical tails, with the horizontal tail being common. In addition, the propulsors were designed so that the rotor, stator, internal ducting, center-body, nozzle, and electric motor comprise a single removable unit that is separate from the outer nacelle and is interchanged between the non-BLI and the BLI configurations. Three propulsor nozzle plugs, shown in Fig. 4, were used to vary the nozzle area and cover a range of propulsive efficiencies that represent different propulsor design choices.

2. *Experimental Data*

Forces and moments on the model were measured using a NASA six-component internal force balance. The forces have the model weight contributions removed using wind-off weight tare measurements to obtain the aerodynamic forces on the entire model, including its propulsors. The uncertainties in net streamwise force and lift coefficients are 3.4×10^{-4} and 0.0028, respectively.

The electrical power input to the model propulsors is converted to mechanical flow power, P_K, via complementary fan and motor characterization experiments. An independent method that uses flow surveys at the inlet and exit of the propulsors to calculate P_K from its definition (3) corroborated the validity of the flow power data.

A minimum of 12 repeat runs were taken for each experimental condition (freestream speed, angle of attack, propulsor power) throughout the two test campaigns to achieve a tight confidence interval. Detailed uncertainty analysis and sensitivities to data processing and modeling assumptions are provided in [9,10].

All the data used in the present paper were taken at $C_L = 0.64$, which occurs at approximately 2° model angle of attack and is the lift coefficient value of the full-scale D8.2 aircraft. The net streamwise force was varied by changing the propulsor power, with the cruise condition defined by $C_X = 0$.

B. Benefit at Equal Nozzle Area

The data obtained with the nominal nozzle area (Plug B) on both configurations are used to quantify the benefit of BLI when the same propulsor is used in non-BLI and BLI installations—a design choice of equal nozzle area.

1. *Force versus Power*

The experimentally measured force versus power data points for each configuration are fit using the parametric expressions (37) and (38) to obtain the power functions for BLI and non-BLI configurations $C'_{P_K}(C'_X)$ and $C'_{P_K}(C'_X)$, respectively. A least-square fitting procedure determines the values for the parameters in these expressions. To sufficiently constrain the fitting, the BLI propulsor jet area is set at the corresponding value for the non-BLI propulsor, that is, $A_{\text{jet}} = A'_{\text{jet}}$. The values of C'_D and $A_{\text{jet}}/A_{\text{nozzle}}$ are determined using the non-BLI data, and then used to fit the BLI data and find $\Delta C_{\Phi_{\text{surf}}}$ and f_{wake}. The jet velocity, V_{jet}/V_∞, varies along the $C_{P_K}(C_X)$ curve.

The values of the parameters obtained from curve-fitting the experimental data are listed in Table 1 and closely match the expected values. For example, $\Delta C_{\Phi_{\text{surf}}} = 0.0012$ is consistent with the smaller nacelle wetted area and lower surface velocities of the BLI configuration. The fit result $f_{\text{wake}} = 0.08$ is close to the 0.09 value obtained from a viscous/inviscid calculation for the D8 fuselage, and the $A_{\text{jet}}/A_{\text{nozzle}}$ ratios are the same as those from a through-flow calculation of the non-BLI propulsor. This gives confidence that the power balance model employed and the few simplifying assumptions introduced are valid.

The $C_{P_K}(C_X)$ curves for the two configurations are plotted in Fig. 5, together with the data points used to generate them. The aerodynamic BLI benefit with equal nozzle area at cruise is determined to be 8.2%. This is slightly lower than the 8.6% value previously obtained using a polynomial fit to the force versus power data [9], but remains within the experimental uncertainty.

The present analysis framework has two important advantages. First, the curve fit to experimental data is excellent across a wider range of power levels (propulsor operating conditions) than a polynomial fit. Second, it is possible to determine intermediate quantities that provide insight into the physical mechanisms behind the performance changes with BLI, as leveraged in the benefit sources analysis of Sec. IV.D.

Table 1 Result of data fits with expressions for force and power for the nominal nozzle area

C'_D	$\Delta C_{\Phi_{\text{surf}}}$	f_{wake}	$A_{\text{jet}}/A_{\text{nozzle}}$
0.0370	0.0012	0.080	0.955

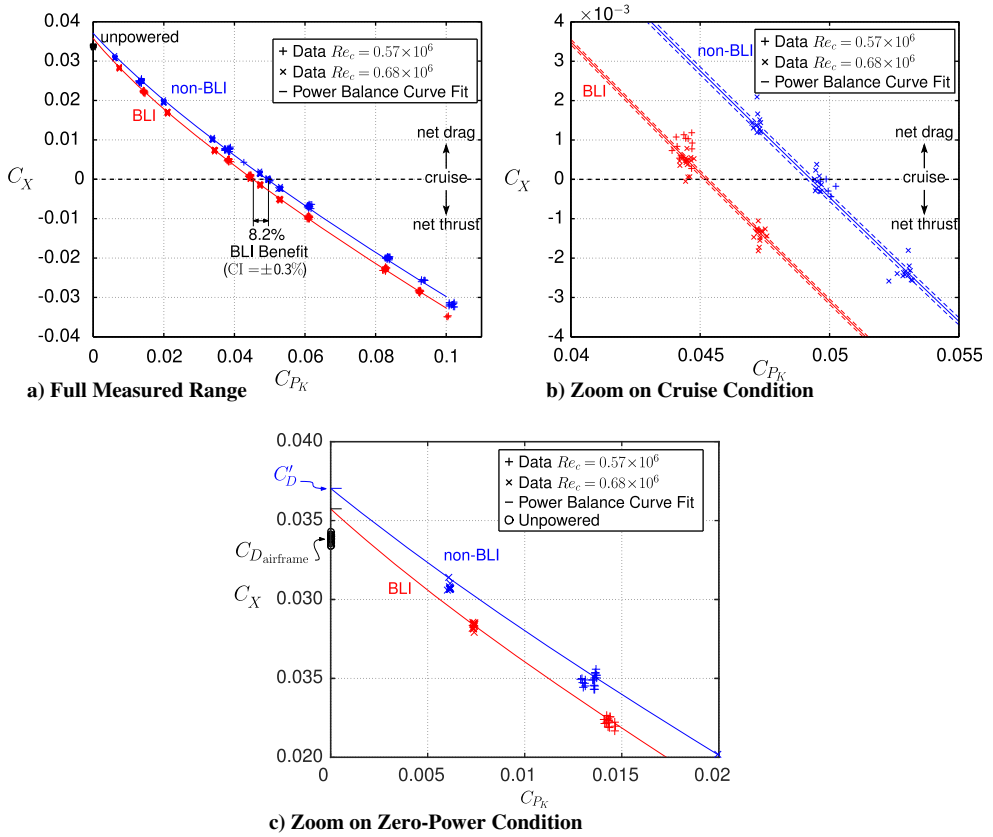

Fig. 5 Net streamwise force coefficient versus mechanical flow power coefficient with nominal nozzle area at cruise C_L: experimental measurements (symbols) and curve fits based on the framework expressions (lines). The dotted lines in subfigure (b) show the size of the 95% confidence interval of the experimental data.

2. *Zero-Power Condition*

The streamwise force on either an unpowered model or a powered model at zero power ($C_{P_K} = 0$) is equivalent to the conventional definition of *drag*. This drag definition is also consistent with the conventions adopted in the derivation of the power-balance parametric expressions in the absence of BLI.

Figure 5c zooms into the $C_{P_K} = 0$ area of the force-power curve and includes the force measured on the unpowered configuration. The unpowered-model streamwise force coefficient is the drag coefficient of the airframe, whose average experimental value is $C_{D_{\text{airframe}}} = 0.0338$. The location where the curve fit for the non-BLI configuration intersects the $C_{P_K} = 0$ axis gives the drag coefficient of the non-BLI configuration $C'_D \equiv C'_X(C'_{P_K} = 0) = 0.0370$. The difference is a measure of the drag of the non-BLI propulsors (pylons and nacelles), $C'_{D_{\text{prop}}} = C'_D - C_{D_{\text{airframe}}} = 0.0032$. Similarly, the C_X difference between BLI and unpowered configurations quantifies the drag of the BLI propulsors (half-nacelles and blending surfaces), $C_{D_{\text{prop}}} = C_{X_0} - C_{D_{\text{airframe}}} = 0.0019$, where $C_{X_0} \equiv C_X(C_{P_K} = 0)$.

The only differences between the BLI and non-BLI geometries are at the level of the propulsion system, and the vortex dissipation was verified to be the same for non-BLI and BLI installations [9]. Therefore, in the absence of jet dissipation such as when $C_{P_K} = 0$, the dissipation difference between configurations is only due to changes in the surface and wake dissipation of the flow streams that pass around the propulsors, that is

$$C'_D - C_{X_0} = C'_{\Phi_{\text{prop}}} - C_{\Phi_{\text{prop}}} \tag{43}$$

Furthermore, propulsors at the cruise angle of attack are very nearly nonlifting and their dissipation is only consisted of surface and wake parts, such that

$$C_{\Phi_{\text{prop}}} = C_{\Phi_{\text{prop,surf}}} + C_{\Phi_{\text{prop,wake}}} = \frac{C_{\Phi_{\text{prop,surf}}}}{1 - f_{\text{wake}}} \tag{44}$$

and it is expected that

$$\begin{aligned}\Delta C_{\Phi_{\text{surf}}} &= C'_{\Phi_{\text{prop,surf}}} - C_{\Phi_{\text{prop,surf}}} \\ &= (1 - f_{\text{wake}})(C'_{\Phi_{\text{prop}}} - C_{\Phi_{\text{prop}}}) \\ &= (1 - f_{\text{wake}})(C'_D - C_{X_0})\end{aligned} \tag{45}$$

The left- and right-hand sides have the same value of 0.0012 (see Tables 1 and 2), and so this equation is indeed verified by the data.

3. *Propulsive Efficiency*

The BLI benefit is partly the result of propulsive efficiency gains. Figure 6 shows the cruise mechanical flow power ratio versus propulsive efficiency with the nominal nozzle area. The lines show curve fits of $1/\eta_p$ to reflect the scaling

$$P_K = \frac{P_K - \Phi_{\text{jet}}}{\eta_p} = \frac{\Phi_{\text{surf}} + \Phi_{\text{wake}} + \Phi_{\text{vortex}}}{\eta_p} \propto \frac{1}{\eta_p} \tag{46}$$

and the error bars give the 95% confidence intervals from the curve fits.

The vertical offset between the BLI and non-BLI curves is the difference in airframe dissipation ($\Phi_{\text{surf}} + \Phi_{\text{wake}} + \Phi_{\text{vortex}}$) between the two configurations. The BLI airframe has 4% less dissipation, due

Table 2 Net streamwise forces at zero power with nominal nozzle area

Configuration	Force at zero power: $C_X(C_{P_K} = 0)$
Unpowered	$C_{D_{\text{airframe}}} = 0.0338$
Non-BLI	$C'_D = 0.0370$
BLI	$C_{X_0} = 0.0357$
	$(1 - f_{\text{wake}})(C'_D - C_{X_0}) = 0.0012$

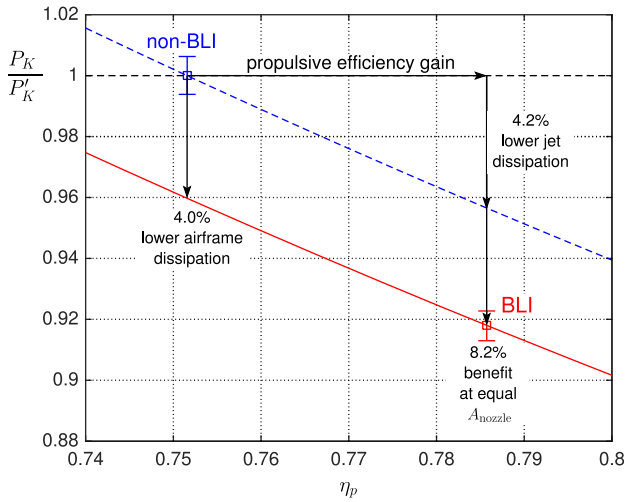

Fig. 6 Mechanical flow power ratio versus propulsive efficiency at cruise with nominal nozzle area: experimental measurements (symbols), confidence intervals (error bars), and curves with $1/\eta_p$ scaling (lines).

to the smaller nacelles and the reduced wake dissipation, as confirmed in Sec. IV.D. The rest of the benefit can be seen as an increase in propulsive efficiency as indicated by the horizontal offset between BLI and non-BLI points. These two contributions add up to the 8.2% benefit at cruise noted previously.

Table 3 Propulsion system parameters for D8 wind tunnel model and full-scale D8.2 aircraft; for the latter, values given are mass averages between fan and core propulsor flows

	BLI model			
	Plug A	Plug B (nominal)	Plug C	Full-scale D8.2 Aircraft
C_{P_K}	0.0445	0.0452	0.0460	0.0421
η_p	0.791	0.786	0.773	0.771
$A_{\text{fan}}/S_{\text{ref}}$		2×0.01461		2×0.01457
$A_{\text{nozzle}}/A_{\text{fan}}$	0.679	0.604	0.535	0.618
V_{jet}/V_∞	1.59	1.60	1.63	1.56
$f_{\text{BLI}}C'_{D_p}$	0.0039	0.0035	0.0027	0.0034

C. Varying Nozzle Area: Different Propulsor Designs

1. Mechanical Flow Power

Given a BLI configuration, there is more than one way to choose a non-BLI propulsor for comparison. This reflects the dependence of expressions (37) and (38) upon a number of parameters, and specifying the same net force is not sufficient to uniquely define a propulsor.

In the wind tunnel tests, a range of possible comparisons was spanned by varying the nozzle area via installation of different size nozzle plugs. As was done for the nominal plug, the experimental data for each plug are fitted using the parametric expressions (37) and (38). All cases use the same value of $f_{\text{wake}} \simeq 0.080$.

The results at cruise for the different plugs are given in Tables 3 and 4. Table 3 also lists propulsor quantities for the full-scale D8.2 aircraft to show that the wind tunnel tests spanned the full-scale characteristics and therefore provide a good representation of what can be expected in flight. The full-scale D8.2 values are conceptual-level estimates using TASOPT [6–8].

Figure 7 shows the power ratio versus propulsive efficiency for the three plugs (nozzle areas) considered. The benefit at equal nozzle area varies from 7.6 to 8.5% depending on the plug. This is shown in Sec. IV.D to be due to changes in the amount of ingested dissipation.

2. Specific Propulsive Power

The specific power versus propulsive efficiency from Eq. (41) is plotted for a range of f_{BLI} values in Fig. 8. It corresponds to the classical propulsive efficiency versus specific power (or thrust) plot [18], extended to include BLI. The points indicate the measured values for wind tunnel models and the estimated full-scale D8.2 performance, while the curves give the predictions based on the expressions of Sec. III.

The figure illustrates the trade-offs in propulsor sizing between high propulsive efficiency and reduced weight with high specific propulsive power. The D8 BLI and non-BLI propulsors have similar specific powers, but the former takes advantage of a higher efficiency

Table 4 BLI and non-BLI configurations cruise characteristics for the D8 wind tunnel tests, and breakdown of the BLI aerodynamic benefit into its sources

		Non-BLI			BLI		
		Plug A	Plug B (nominal)	Plug C	Plug A	Plug B	Plug C
Power quantities	C_{P_K}	0.0482	0.0493	0.0502	0.0445	0.0452	0.0460
	PSC $= 1 - P_K/P'_K$	— —	— —	— —	**7.6%**	**8.2%**	**8.5%**
Dissipation quantities	C'_D	0.0364	0.0370	0.0374	— —	— —	— —
	$C_{\Phi_{\text{vortex}}}$			0.0084			
	$C_{\Phi_{\text{jet}}}$	0.0118	0.0122	0.0128	0.0093	0.0097	0.0104
	$(C_{\Phi_{\text{jet}}} - C'_{\Phi_{\text{jet}}})/(C_{P_K} - C'_{P_K})$	— —	— —	— —	**69%**	**63%**	**57%**
	$C_{\Phi_{\text{wake}}}$	0.0022	0.0023	0.0023	0.0019	0.0020	0.0021
	$(C_{\Phi_{\text{wake}}} - C'_{\Phi_{\text{wake}}})/(C_{P_K} - C'_{P_K})$	— —	— —	— —	**8%**	**7%**	**5%**
	$C_{\Phi_{\text{surf}}}$	0.0257	0.0263	0.0266	0.0249	0.0251	0.0250
	$(C_{\Phi_{\text{surf}}} - C'_{\Phi_{\text{surf}}})/(C_{P_K} - C'_{P_K})$	— —	— —	— —	**23%**	**30%**	**38%**
	$\Delta C_{\Phi_{\text{surf}}}$	— —	— —	— —	0.0008	0.0012	0.0016
	$f_{\text{BLI}}C'_{D_p}$	0	— —	— —	0.0039	0.0035	0.0027
	f_{BLI}	0	— —	— —	**0.140**	**0.122**	**0.092**
Propulsor quantities	V_{jet}/V_∞	1.65	1.66	1.69	1.59	1.60	1.63
	$A_{\text{jet}}/A_{\text{nozzle}}$	0.856	0.955	1.031	0.856	0.955	1.031
	$A_{\text{nozzle}}/A_{\text{fan}}$	0.679	0.604	0.535	0.679	0.604	0.535
	V_{fan}/V_∞	0.959	0.958	0.930	0.922	0.923	0.899
	ϕ	0.351	0.346	0.341	0.348	0.344	0.334
	η_p	0.755	0.752	0.744	0.791	0.786	0.773
	η_p/η'_p	— —	— —	— —	1.048	1.045	1.039
	$C_{P_{\text{sp}}}$	0.649	0.661	0.688	0.653	0.659	0.676

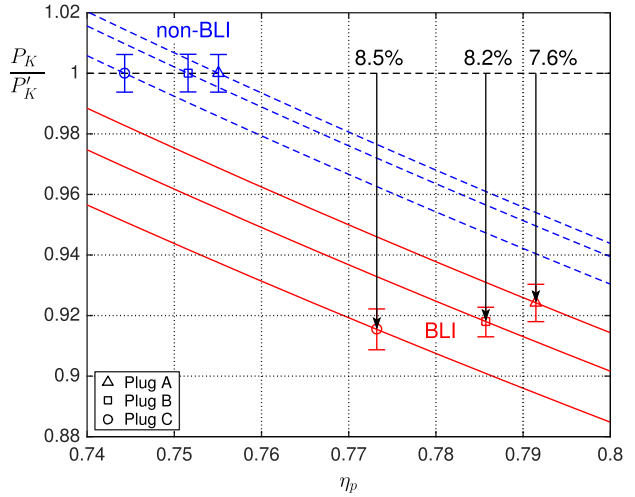

Fig. 7 Mechanical flow power ratio versus propulsive efficiency at cruise: experimental measurements (symbols), confidence intervals (error bars), and curves with $1/\eta_p$ scaling (lines).

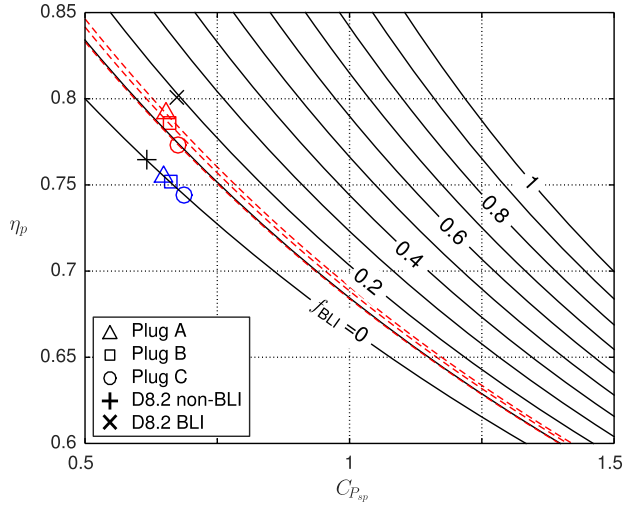

Fig. 8 Propulsive efficiency versus specific propulsive power of non-BLI and BLI configurations at cruise: experimental measurements (closed symbols), full-scale D8.2 aircraft predictions (open symbols), and curves based on framework expressions (lines).

as evidenced by the upward shift in the curves with increasing f_{BLI}. BLI enables the production of useful (propulsive) power at a higher efficiency than does a conventional non-BLI propulsion system.

D. Sources of BLI Benefit

To quantify the sources of the aerodynamic BLI benefit, the dissipation components in the nondimensional form of the power balance equation (1),

$$C_X = C_{\Phi_{\text{jet}}} + C_{\Phi_{\text{surf}}} + C_{\Phi_{\text{wake}}} + C_{\Phi_{\text{vortex}}} - C_{P_K} \tag{47}$$

are computed at the cruise condition ($C_X = 0$) for each nozzle area via their respective expressions from Sec. III.A. The parameters C'_D, $\Delta C_{\Phi_{\text{surf}}}$, and $A_{\text{jet}}/A_{\text{nozzle}}$ for each case are obtained from the curve fits to the experimental data, and $C'_{D_p} = C'_D - C_{\Phi_{\text{vortex}}}$ is computed from (23) using $C_L = 0.64$, $AR = 15.43$, and $e = 1$ as determined in [9]. The ratio V_{jet}/V_∞ is the parameter in the $C_{P_K}(C_X)$ expressions that sets the propulsor operating point. Its cruise value is found by setting C_X to zero, and is then used to compute the jet dissipation via Eq. (28). The resulting dissipation components are given in Table 4 and identify the origins of the BLI benefit.

The aerodynamic benefit of BLI is composed of the following, which provide the breakdown of the benefit into its sources:

1) Between 57 and 69% (nominally 63%) of the benefit is due to a decreased jet dissipation with BLI, and the associated increase in propulsive efficiency, as indicated by the values of $(C_{\Phi_{\text{jet}}} - C'_{\Phi_{\text{jet}}})/(C_{P_K} - C'_{P_K})$ in Table 4 and the horizontal offset between BLI and non-BLI points with the same plug in Fig. 7. Lower jet velocity is possible with BLI because the ingested flow is slower ($V_{\text{fan}}/V_\infty < V'_{\text{fan}}/V_\infty$): the same streamwise force, or momentum flux through the propulsor, is thus achieved with a lower jet velocity ($V_{\text{jet}}/V_\infty < V'_{\text{jet}}/V_\infty$). The result is less kinetic energy being lost via jet dissipation ($C_{\Phi_{\text{jet}}} < C'_{\Phi_{\text{jet}}}$), and a more efficient use of the power input. The propulsive efficiency gains between 4 and 5% with BLI at equal nozzle area, or roughly 3.4 percentage points.

2) The BLI benefit is also related to a reduction in surface dissipation, which amounts to between 23 and 38% of the aerodynamic benefit. Compared with a non-BLI installation, the BLI configuration has smaller nacelles with lower surface velocities, with the propulsor in relatively slower boundary layer flow compared with non-BLI pods in freestream. The reduction in surface dissipation, $\Delta C_{\Phi_{\text{surf}}}$, depends on the specifics of the integration between propulsor, fuselage, and vertical tails. Changing nozzle area changes the jet velocity and therefore modifies the flow around the nacelles, thus changing nacelle dissipation. This effect is seen directly in the variation in non-BLI airframe dissipation (or drag) C'_D when plugs are changed. A smaller nozzle areas result in more surface dissipation reduction with BLI, while decreasing nozzle area had detrimental effect on propulsive efficiency.

3) BLI propulsors partially eliminate the fuselage viscous wake, reducing the wake dissipation and contributing between 5 and 8% of the BLI benefit. This wake reduction benefit is directly proportional to the amount of dissipation being ingested per Eq. (20).

Curve-fitting the experimental data with the expressions for C_{P_K} and C_X only determines the amount of dissipation ingested by the propulsors, $f_{\text{BLI}}C'_{D_p}$. However, because C'_D is known from the fitting of the non-BLI data and the vortex dissipation (or induced drag portion) can be estimated from lift coefficient measurements, it is possible to determine C'_{D_p} for each plug and therefore deduce the value of f_{BLI} for each nozzle area, as given in Table 4.

The dissipation ingested by the propulsors varies depending on the propulsor nozzle area. A smaller nozzle area (Plug C) results in increased jet velocity, reduced propulsor mass flow, a smaller propulsor captured streamtube, and therefore less of the fuselage boundary layer being ingested. The ingestion fraction thus decreases with decreasing nozzle area. As a result, when nozzle area is decreased, the parts of the BLI benefit that are proportional to the amount of ingestion, namely, jet- and wake-related parts, become smaller, while the part of the benefit from surface dissipation reduction increases. The balance of this trade-off is a higher aerodynamic benefit for smaller nozzles for the D8 cases tested.

E. BLI Benefit Range: Bases for Comparison

Expressions (37) and (38) can be thought of as a parametric $C_{P_K}(C_X)$ function in which V_{jet}/V_∞ is an independent parameter. Thus, for a given non-BLI propulsor, there is no unique way to choose an equivalent BLI propulsor for comparison, and therefore there is no unique power ratio P_K/P'_K and no unique corresponding BLI benefit. Furthermore, the chosen V'_{jet} and V_{jet} parameter values affect engine size and weight, and thus affect the overall system-level benefit of BLI.

Specific comparisons between BLI and non-BLI propulsor installations can be made at equal mass flow, equal nozzle area, equal jet velocity, equal propulsive efficiency, equal jet dissipation, or equal power. The BLI benefit is manifested differently for each comparison, as Fig. 9 shows using the D8 experimental data and the lines defined by this paper's analysis framework. With constant nozzle area for example, a BLI configuration with $f_{\text{BLI}} = 0.12$ requires roughly 8% less propulsive power than the non-BLI one (Plug B case). If instead the comparison is made at equal propulsor mass flow, the BLI benefit amounts to a 9% power reduction. A benefit of 6% is found with the same jet velocities, and of 4% at the

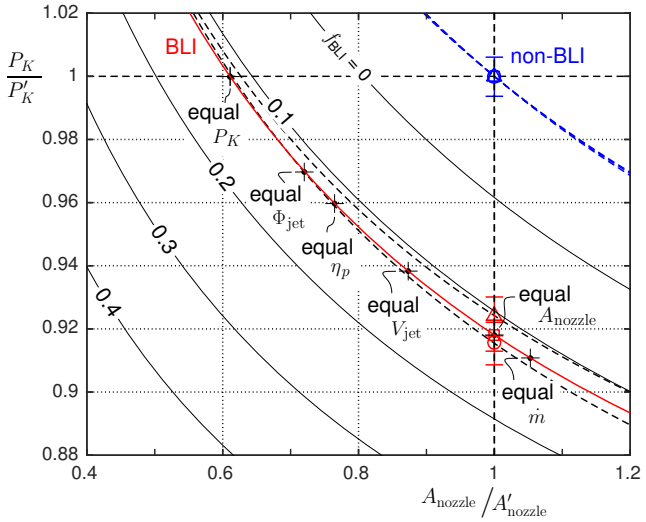

Fig. 9 Range of possible BLI propulsors: cruise power versus nozzle area relative to a reference non-BLI propulsor: experimental measurements (symbols) and curves from framework expressions (lines).

same propulsive efficiency. At the extreme, the BLI propulsor that requires the same power as the non-BLI reference has a nozzle with 40% less area, which represents a smaller engine with a system-level weight benefit.

Note that the $f_{BLI} = 0$ curve in Fig. 9 does not pass through the non-BLI data point at (1,1). Instead there is an offset due to the difference in airframe dissipation between non-BLI and BLI installations.

These trade-offs emphasize that the aerodynamic benefit of BLI is only part of the story: there are important choices to be made when designing a BLI aircraft for aerodynamic performance, and there are additional system-level weight benefits enabled by adopting a BLI propulsion system. The optimal BLI aircraft needs to be designed to take maximum advantage of the various benefits of BLI. Figure 9 and the expressions derived in this paper provide a framework for analyzing aircraft with BLI.

It is worth noting that the expressions derived in Sec. III are based on the assumption of a uniform jet velocity. The excellent match between the D8 wind tunnel measurements and what the expressions predict further supports this assumption.

V. Conclusions

This paper determines the sources of the aerodynamic benefit due to boundary layer ingestion (BLI). This benefit is defined as the reduction in mechanical flow power required with BLI to produce a given net streamwise force relative to a non-BLI aircraft with the same airframe and operating at the same lift coefficient. It is due to, in order of importance, 1) reduced jet dissipation and hence increased propulsive efficiency; 2) reduced surface dissipation from nacelles with smaller wetted area and lower surface velocities; and 3) reduced wake dissipation from partial wake removal through ingestion.

A framework for evaluating aircraft performance in the presence of BLI is introduced. Parametric expressions for the input mechanical flow power and resulting steamwise force on an aircraft are derived based on the power balance method. They explicitly quantify the performance of a BLI aircraft as a function of the total and profile drag of an equivalent non-BLI configuration and of BLI design quantities. Expressions for the dissipation components with and without BLI determine the breakdown of the benefit into its the sources.

It is shown that the aerodynamic benefit is not unique, but rather depends on how the baseline non-BLI configuration is selected, with the specific benefit of BLI depending on how the comparison is made (e.g., at equal engine nozzle area, mass flow, or other). Our model indicates that the magnitude of the benefit is determined by three major parameters: the amount of dissipation ingested by the propulsors; the propulsor jet velocity (usually set by the propulsor mass flow or operating point); and how efficient the BLI installation is (as reflected in surface dissipation reductions).

The BLI analysis framework is applied to the D8 powered wind tunnel tests performed on configurations with and without BLI in the NASA Langley 14- by 22-Foot Subsonic Tunnel. When comparison between BLI and non-BLI is made at equal nozzle area (i.e., use of the same propulsors on both configurations), BLI reduces the cruise power requirement by between 7.6 and 8.5%, with the BLI propulsors that ingest between 9 and 14% of the total airframe dissipation. This benefit is found to be broken down as follows: 57–69% of it is due to lower jet dissipation (with a roughly 3 percentage points higher propulsive efficiency); 23–38% is associated with a lower nacelle surface dissipation; and the remaining 5–8% is the result of a lower wake dissipation.

If the comparison between BLI and non-BLI installations is made at equal propulsor mass flow, the aerodynamic BLI benefit for the D8 amounts to a 9% power reduction. The benefit is 6% with the same jet velocities and 4% at the same propulsive efficiency. These numbers refer to aerodynamic benefit alone and there can be additional system-level benefits: for instance, a BLI propulsor that uses the same amount of power as one without BLI would be roughly 40% smaller in size and therefore significantly lighter.

The modeling framework presented in this paper was applied to subscale, low-speed data in Sec. IV. At full scale the numerical values of the various parameters will change. However, because the modeling equations do not have any Reynolds number dependence, the model will remain valid for full-scale aircraft. Compressibility effects would be accounted for by including the P_V term as discussed in Sec. II.B.

This paper introduced a general methodology that can be used to determine the aerodynamic performance gains that BLI provides for an aircraft and to define the sources of these gains. As such, it should be useful in conceptual level and higher-fidelity analyses of aircraft with BLI.

Acknowledgments

This work was partly supported by the NASA Fundamental Aeronautics Program, Fixed Wing Project (now Advanced Air Vehicles Program, Advanced Air Transport Technology Project) through Cooperative Agreement Number NNX11AB35A as part of the MIT $N + 3$ Phase 2 program. The authors are pleased to acknowledge contributions from the rest of the MIT $N + 3$ team and from our partners at Aurora Flight Sciences and Pratt & Whitney, who participated in the design and execution of the D8 wind tunnel tests. We would like to thank in particular Michael Lieu, Nina Siu, Neil Titchener, and Cécile Casses, who were part of the team's core. We are also most indebted to the contributions from Greg Gatlin and Judith Hannon of NASA Langley who were instrumental to the success of the tests.

References

[1] Liebeck, R. H., "Design of the Blended Wing Body Subsonic Transport," *Journal of Aircraft*, Vol. 41, No. 1, 2004, pp. 10–25. doi:10.2514/1.9084

[2] Kawai, R., Friedman, D., and Serrano, L., "Blended Wing Body (BWB) Boundary Layer Ingestion (BLI) Inlet Configuration and System Studies," NASA CR-2006-214534, 2006.

[3] Felder, J. L., Kim, H. D., Brown, G. V., and Chu, J., "An Examination of the Effect of Boundary Layer Ingestion on Turboelectric Distributed Propulsion Systems," *AIAA SciTech, 49th Aerospace Sciences Meeting*, AIAA Paper 2011-0300, Jan. 2011.

[4] Wick, A. T., Hooker, J. R., Hardin, C. J., and Zeune, C. H., "Integrated Aerodynamic Benefits of Distributed Propulsion," *AIAA SciTech, 53rd Aerospace Sciences Meeting*, AIAA Paper 2015-1500, Jan. 2015.

[5] Welstead, J., and Felder, J., "Conceptual Design of a Single-Aisle Turboelectric Commercial Transport with Fuselage Boundary Layer Ingestion," *AIAA SciTech, 54th Aerospace Sciences Meeting*, AIAA Paper 2016-1027, Jan. 2016.

[6] Greitzer, E. M., Bonnefoy, P., De la Rosa Blanco, E., Dorbian, C., Drela, M., Hall, D., Hansman, R., Hileman, J., Liebeck, R., and Lovergren, J., "$N + 3$ Aircraft Concept Designs and Trade Studies, Final Report," NASA CR 2010-216794, 2010.

[7] Drela, M., "Development of the D8 Transport Configuration," *29th AIAA Applied Aerodynamics Conference*, AIAA Paper 2011-3970, June 2011.
[8] Uranga, A., Drela, M., Greitzer, E. M., Titchener, N. A., Lieu, M. K., Siu, N. M., Huang, A. C., Gatlin, G. M., and Hannon, J. A., "Preliminary Experimental Assessment of the Boundary Layer Ingestion Benefit for the D8 Aircraft," *AIAA SciTech, 52nd Aerospace Sciences Meeting*, AIAA Paper 2014-0906, Jan. 2014.
[9] Uranga, A., Drela, M., Greitzer, E., Hall, D., Titchener, N., Lieu, M., Siu, N., Huang, A., Gatlin, G., and Hannon, J., "Boundary Layer Ingestion Benefit of the D8 Aircraft," *AIAA Journal*, Vol. 55, No. 11, 2017, pp. 3693–3708. doi:10.2514/1.J055755
[10] Uranga, A., Greitzer, E., Drela, M., Casses, C., DiOrio, D., Espitia, A., Grasch, A., Hall, D., Huang, A., and Lieu, M., "Aircraft and Technology Concepts for an $N + 3$ Subsonic Transport, Phase 2 Final Report," GTL Rept. Series 2, No. 2.001, Gas Turbine Lab., Massachusetts Inst. of Technology, Cambridge, MA, May 2018.
[11] Drela, M., "Power Balance in Aerodynamic Flows," *AIAA Journal*, Vol. 47, No. 7, 2009, pp. 1761–1771. doi:10.2514/1.42409
[12] Hall, D. K., Huang, A. C., Uranga, A., Greitzer, E. M., Drela, M., and Sato, S., "Boundary Layer Ingestion Propulsion Benefit for Transport Aircraft," *Journal of Propulsion and Power*, Vol. 33, No. 5, 2017, pp. 1118–1129. doi:10.2514/1.B36321
[13] Smith, A. M. O., and Roberts, H. E., "The Jet Airplane Utilizing Boundary Layer Air for Propulsion," *Journal of the Aeronautical Sciences*, Vol. 14, No. 2, 1947, pp. 97–109. doi:10.2514/8.1273
[14] Smith, L., "Wake Ingestion Propulsion Benefit," *Journal of Propulsion and Power*, Vol. 9, No. 1, 1993, pp. 74–82. doi:10.2514/3.11487
[15] Betz, A., *Introduction to the Theory of Flow Machines*, 1st English ed., Pergamon Press, New York, 1966, Chap. 59.
[16] Sato, S., "The Power Balance Method for Aerodynamic Performance Assessment," Ph.D. Thesis, Massachusetts Institute of Technology, Cambridge, MA, June 2012, http://hdl.handle.net/1721.1/75837.
[17] Drela, M., and Giles, M., "Viscous-Inviscid Analysis of Transonic and Low Reynolds Number Airfoils," *AIAA Journal*, Vol. 25, No. 10, 1987, pp. 1347–1355. doi:10.2514/3.9789
[18] Kerrebrock, J., *Aircraft Engines and Gas Turbines*, MIT Press, Cambridge, MA, 1977, Chap. 1.

B. Ganapathisubramani
Associate Editor